

# Composable Visual Tokenizers with Generator-Free Diagnostics of Learnability

**Bingchen Zhao**<sup>1,2</sup>, **Qiushan Guo**<sup>1</sup>, **Ye Wang**<sup>1</sup>, **Yixuan Huang**<sup>1</sup>  
**Zhonghua Zhai**<sup>1</sup>, **Yu Tian**<sup>1,†</sup>

<sup>1</sup>ByteDance Seed, <sup>2</sup>University of Edinburgh

†Corresponding authors

## Abstract

We introduce COMPTOK, a training framework for learning visual tokenizers whose tokens are enhanced for compositionality. COMPTOK uses a token-conditioned diffusion decoder. By employing an InfoGAN-style objective, where we train a recognition model to predict the tokens used to condition the diffusion decoder using the decoded images, we enforce the decoder to not ignore any of the tokens. To promote compositional control, besides the original images, COMPTOK also trains on tokens formed by swapping token subsets between images, enabling more compositional control of the token over the decoder. As the swapped tokens between images do not have ground truth image targets, we apply a manifold constraint via an adversarial flow regularizer to keep unpaired swap generations on the natural-image distribution. The resulting tokenizer not only achieves state-of-the-art performance on image class-conditioned generation, but also demonstrates properties such as swapping tokens between images to achieve high level semantic editing of an image. Additionally, we propose two metrics that measures the landscape of the token space that can be useful to describe not only the compositionality of the tokens, but also how easy to learn the landscape is for a generator to be trained on this space. We show in experiments that COMPTOK can improve on both of the metrics as well as supporting state-of-the-art generators for class conditioned generation.

**Date:** February 4, 2026

**Correspondence:** Bingchen Zhao at [zhaobc.gm@gmail.com](mailto:zhaobc.gm@gmail.com), Yu Tian at [tianyu0124@gmail.com](mailto:tianyu0124@gmail.com)

## 1 Introduction

Visual tokenizers define the representation space in which modern image generators operate. Most established tokenizers produce 2D latent grids, spatial feature maps that preserve locality and are naturally consumed by convolutional or U-Net style decoders. Increasingly, however, recent work has explored 1D token sequences that linearize visual content into a list of tokens, motivated by tighter integration with transformer-based priors [42], flexible rate allocation [1], and a more “language-like” interface for autoregressive modeling and editing [36]. This shift raises a foundational question: what properties should a tokenizer’s tokens satisfy in order to serve as a reliable representation space for generation and manipulation?

For tokenizers to be broadly useful beyond reconstruction, their tokens should satisfy two properties. First, token usefulness: each token (or token group) should carry non-trivial, usable information about the image,

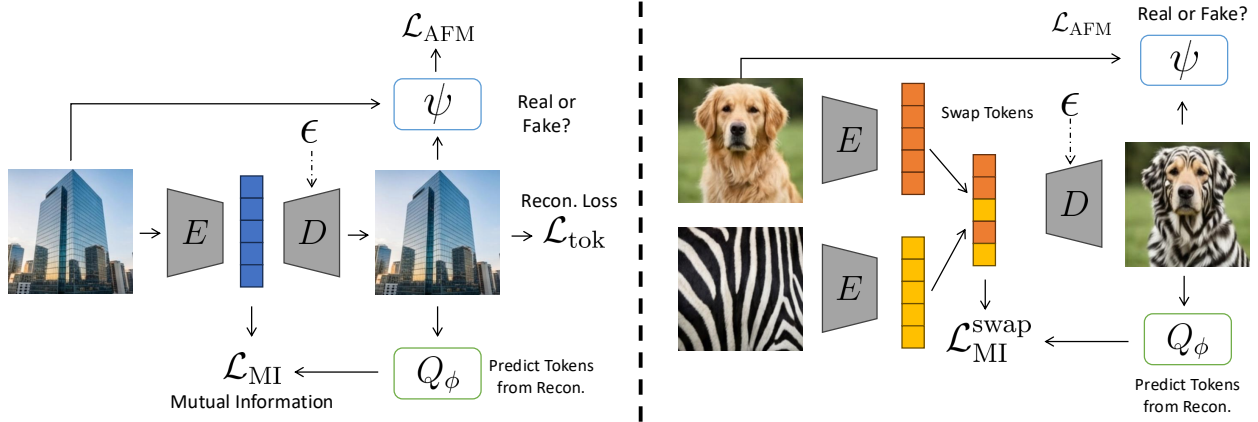


**Figure 1** COMPTOK overview. Left: a reconstruction pathway where the encoder  $E$  produces a 1D token sequence that is decoded by  $D$ ; a recognition head  $Q_\phi$  must recover the tokens from the decoded image (mutual-information loss  $\mathcal{L}_{\text{MI}}$ ), while an adversarial flow/density model  $\psi$  enforces realism via  $\mathcal{L}_{\text{AFM}}$  alongside the reconstruction loss  $\mathcal{L}_{\text{tok}}$ . Right: a swap pathway where tokens from two images are partially exchanged, the mixed token is decoded, and the same recoverability and realism constraints  $\mathcal{L}_{\text{MI}}^{\text{swap}}$  and  $\mathcal{L}_{\text{AFM}}$  train tokens to be non-degenerate and compositional under edits.

rather than being redundant given other tokens [45]. Prior works [45] studied that the utilization of codebooks matters for the performance of tokenizers, indicating that we need the tokens to carry as much of useful information as possible. Second, token compositionality: tokens should behave as stable control variables, swapping or editing a subset of tokens should yield predictable changes while keeping the decoded image on the natural-image manifold. Beyer et al. [2] shows that 1D tokenizers can be used directly for generation tasks because it is highly compressed so the tokens can demonstrate stable control over the image. These properties directly determine whether the token from the tokenizer can support training of generators for fine-grained control and modular editing.

We study 1D tokenizers in this work, as they are the instances where the tokens carry semantic level information over the images rather than patch level information [2, 36, 42]. Existing work has largely optimized 1D tokenizers for rate–distortion [42] and modeling efficiency [30, 45], and has demonstrated that imposing structure can yield strong generation with relatively few tokens [1, 36]. This is valuable, but it also highlights what is missing: current evaluations and training objectives do not explicitly enforce that all tokens remain causally effective and compositional. In other words, the tokenizers can learn highly entangled tokens under these constraints, and these complex interactions between tokens can make it hard for generators to learn on the token space. As a result, reconstruction fidelity can be a poor predictor of generative performance and of controllability as shown in prior works [38]: a tokenizer may reconstruct well yet induce a latent space whose “usable region” is fragmented or whose subset of tokens are effectively ignored by the generator [1, 36].

In this work, we propose COMPTOK, a 1D tokenizer training framework designed to produce compositional tokens that provides a easier to learn landscape for the generators. COMPTOK leverages a diffusion-based decoder following prior works [1, 36] as this is able to decouple the frequency information from the tokens [36]. Additionally, COMPTOK uses an InfoGAN-style loss that requires the decoded images from the decoder can be used by a recognition model to predict the exact tokens the images is decoded from. This requires the tokens to be learned in a causally effective manner where the decoder cannot ignore them, otherwise it will get penalized. To further strength the compositional control of tokens over the decoder, the decoder of COMPTOK trains on tokens formed by swapping token subsets between images, and enforces realism for these compositions of tokens via a manifold constraint implemented with an adversarial flow regularizer [21]. This swap-regularized training expands the set of valid token compositions and strengthens the interventional effect of tokens, enabling strong performance in class-conditioned image generation.

Our second contribution is a pair of metrics for tokenizer usability that go beyond reconstruction fidelity. Average information gain (AvgIG) measures how reconstruction progress is distributed during latent optimization starting with a random token to reconstruct a given input image. AvgIG measures on average, how

much information is gained by each step of optimization. If the landscape is flat around a real token, AvgIG will be small as optimization gains less information at each step. This implies the decoder is ignoring token changes, a phenomenon we term Token Neglect. Consequently, a higher AvgIG is desirable to ensure the decoder remains sensitive to token changes, thereby guaranteeing that every token contributes effectively. Mode connectivity (MC) characterizes latent geometry by measuring whether high-quality real tokens, and critically, mixed tokens produced by token swapping, lie in a connected, low-barrier region, indicating whether the representation is learnable for a generator and stable under compositional edits. If the landscape has high walls or spikes between two valid real tokens, the space is fragmented. This makes it impossible for a generator to interpolate or transition between concepts encoded by different tokens. A higher MC would indicate that the representation avoids fragmentation and is stable under compositional edits. Crucially, these metrics are complementary: AvgIG ensures the “basins” of the loss landscape are steep and well-defined (preventing token neglect), while MC ensures these basins are connected by smooth, low-loss paths (preventing manifold artifacts).

Empirically, we evaluate tokenizers built from diverse methods [34, 44]. We show that AvgIG and MC have substantial predictive power for downstream generation and control, and that COMPTOK consistently improves both metrics and generative performance—demonstrating that practical tokenizer quality is governed not only by reconstruction, but by token utilization and the geometry of compositional latent space.

## 2 Related Work

**Image tokenization for efficient generative modeling.** Visual tokenizers compress images into latent tokens that make training and sampling feasible for large generators. Classical approaches include VAEs [16] and VQ-VAE [34], which introduced a learnable codebook for mapping images to discrete tokens. Subsequent work improved perceptual fidelity and sample sharpness via adversarial and perceptual losses [9] and increased representational capacity via multi-stage or residual quantization [17]. Codebook under-utilization and commitment pathologies have been actively studied; MAGVIT-v2 [40] proposes Look-up Free Quantization (LFQ) to mitigate these issues. More recent tokenizers modernize architectures and training losses, including binary quantization and large-scale conditional generation [35] and scaling studies for ViT-based tokenizers [7, 11]. A complementary line leverages pretrained visual foundation models (e.g., CLIP/MAE/DINOv2) to enrich token semantics or stabilize training [12, 22, 25, 37, 45].

**From 2D grids to 1D causal token sequences.** Many tokenizers produce 2D grids of latent tokens aligned to spatial patches, which is convenient for convolutional decoders but does not directly provide a causal ordering for autoregressive modeling. Several works propose 1D tokenizations that impose a causal dependency, enabling LLM-style decoding for images and more natural integration with autoregressive backbones. TiTok [42] and SEED [10] are representative early 1D tokenizers; subsequent work studies how causal ordering benefits autoregressive modeling [26]. VAR [31] reframes visual AR modeling as next-scale prediction and introduces a multi-scale residual quantization tokenizer that produces low-to-high resolution codes. Adaptive-length tokenization has also been explored, where token budget depends on image content or downstream needs [8]. These directions largely optimize for compression, reconstruction, and likelihood under a chosen generator, while the meaning and controllability of individual tokens remain less explicitly constrained.

**Token usefulness and controllable manipulation.** A recurring practical gap is that strong reconstructions do not guarantee that tokens are beneficial for a downstream generator [38], nor that token edits stay on the natural-image manifold [2]. Prior work on ordered tokens [1, 36] demonstrates that token prefixes can suffice for generation and can improve efficiency, but such results do not directly address our objective: we treat tokens as compositional control variables and prioritize (i) non-degeneracy (each token has interventional effect) and (ii) validity under mixing (swaps remain realistic and stable). COMPTOK differs in that it explicitly targets token usefulness and compositionality through training objectives and diagnostics, rather than focusing primarily on adaptive budget or prefix sufficiency.

**Diffusion and autoregressive generators with token conditioning.** Modern high-fidelity image generators are dominated by diffusion-based models [6, 14, 23, 29] and large autoregressive models [30, 32, 33]. Latent diffusion [27] popularized performing diffusion in the latent space of a pretrained tokenizer [9], substantially

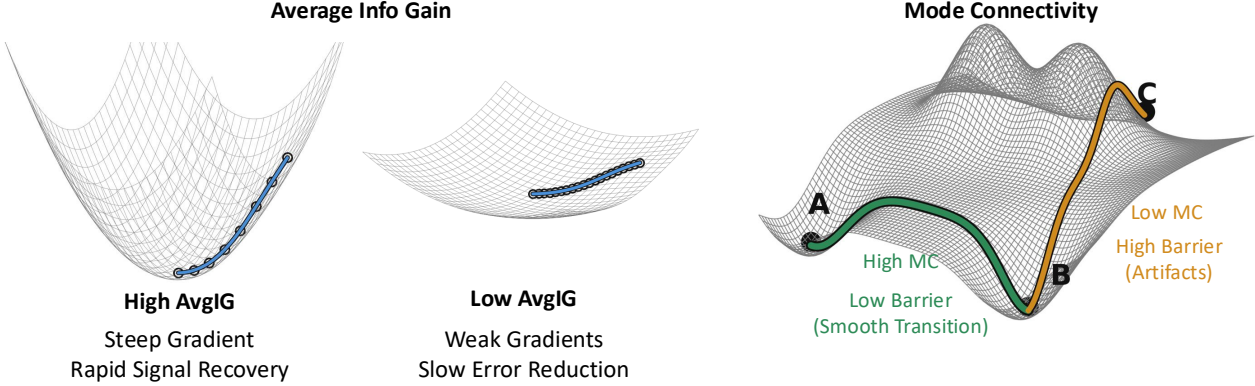


**Figure 2** AvgIG and MC are computed on the tokenizer (E,D) to evaluate the quality of the tokenizer and the downstream generator. AvgIG measures the average information gain per optimization step when fitting a latent token to a target image, and MC measures the pairwise mode connectivity of the tokenizer token space. MC is a measure of the local geometric smoothness of the tokenizer token space.

reducing compute and enabling scalable text/image-conditional generation. Autoregressive approaches require an ordering over tokens; both fixed orderings and randomized orders have been explored [3, 19, 41]. These models typically assume a tokenizer as a front-end, which provides the data distribution to train the generation model on. COMPTOK is a tokenizer and aim to make the tokenizer directly token neglect and encourage compositional control, aiming to improve downstream generation and editing rather than reconstruction alone.

### 3 Method

#### 3.1 Problem Setting

We study a two-stage pipeline: a learned visual tokenizer and a downstream conditional generator trained on the tokenizer’s token space. The tokenizer consists of an encoder-decoder pair (E,D) mapping images  $x \in \mathcal{X}$  to a structured latent token  $z \in \mathcal{Z}$  and back:  $z = E(x)$ ,  $\hat{x} = D(z)$ . We represent the token as a 1D token sequence (or token groups)  $z = (z_1, \dots, z_K)$ , and we do not perform vector quantization following Wen et al. [36]. We use  $\mathcal{X}$  to denotes the full space of all real images, and in practice for training tokenizers we would have a dataset  $\mathcal{D}$  to sample data from. In this paper, D is implemented as a diffusion-based decoder that reconstructs  $x$  conditioned on  $z$ , following prior diffusion-decoder tokenizers [36]. Concretely, D is trained to reconstruct  $x$  from  $z$  via a conditional denoising objective [14].

Separately, we train a downstream generator G on the token space produced by the tokenizer. G can be an image generator conditioned on class labels or text, generating the image tokens to be decoded by D for pixels. Critically, G is not part of the tokenizer. It is trained after (E,D) and its success depends on the quality and geometry of the token space  $\mathcal{Z}$  induced by the tokenizer.

The most common evaluations on (E,D) are to measure the Fréchet Inception Distance (FID) of the reconstructed images [13] to a reference set. The evaluation on G is done similarly by measuring the FID of the generated images by sampling from G conditioned on class labels. We term the FID of the reconstructed images as rFID and the FID of the generated images as gFID.

#### 3.2 Why rFID Can Mislead on gFID

A central empirical issue is that tokenizer reconstruction quality (e.g., rFID of  $D(E(x))$ ) is not always predictive of downstream generation quality of G [11, 38]. Our core view is that rFID evaluates reconstructions only on the encoder manifold on a test dataset  $\mathcal{M}_E = \{E(x) : x \sim \mathcal{D}_{\text{test}}\}$ . However, G must learn a distribution over valid tokens and produce high-quality images from them. This introduces two failure modes that rFID does not directly probe: (1) Token-space completeness of the decoder D. Even if E is fixed, rFID does not separate whether D has the capacity to faithfully reconstruct the target distribution for arbitrary valid tokens. If good reconstructions require finely tuned tokens that occupy a thin set that only  $E$  can generate, then G faces a difficult support-learning problem. (2) Learnability / geometry of the good-token region. If high-quality

tokens form multiple disconnected pockets or have high barriers between modes, then a generator  $G$  trained on tokens will struggle to model this geometry. This yields a mismatch between the token distribution that  $G$  can learn and the tokens that decode well, leading to degraded gFID even when rFID is strong. These observations motivate an evaluation framework for the tokenizer that predicts the downstream potential of  $G$  without training  $G$ .

### 3.2.1 Metrics: AvgIG and MC

We introduce two metrics for tokenizer quality that go beyond reconstruction-only metrics such as rFID. Standard reconstruction metrics evaluate samples only on the encoder manifold; they do not measure whether the token space forms a geometry that a downstream generator can actually learn. Our metrics address this by probing two complementary properties: **AvgIG** ensures the decoder is locally sensitive to tokens, while **MC** ensures the latent manifold is globally connected. Both are computed without training the downstream generator  $G$ .

**AvgIG:** This metric quantifies the “vertical” steepness of the loss landscape, measuring how much usable information the diffusion decoder  $D$  can absorb per optimization step towards reconstructing an image from a random latent token. Intuitively, for tokens to be causally effective, the decoder must be highly sensitive to their values. If decoding is well-conditioned, optimization should yield a rapid reduction in reconstruction error, indicating that the information in the tokens  $z$  is actionable and accessible, a prerequisite for downstream learning.

**Definition.** Fix the diffusion decoder  $D$  and a target image  $x$ . Starting from an initialization  $z^0$ , we optimize the latent token by gradient descent on MSE:

$$\begin{aligned} z^{t+1} &= z^t - \eta \nabla_z \frac{1}{2} \|D(z^t) - x\|_2^2 \\ \text{MSE}_t &= \frac{1}{N} \|D(z^t) - x\|_2^2, \end{aligned} \quad (1)$$

where  $N$  is the number of pixels. We define the per-step information gain (in bits):

$$\begin{aligned} \Delta I_t(x) &= \frac{N}{2} \log_2 \left( \frac{\text{MSE}_t}{\text{MSE}_{t+1}} \right) \\ \text{AvgIG} &= \mathbb{E}_{x \sim \mathcal{D}} [\Delta I_t(x)]. \end{aligned} \quad (2)$$

AvgIG measures the efficiency of signal recovery. A low AvgIG implies weak gradients or flat local plateaus where changing  $z$  has little effect on  $D(z)$ , a symptom of token neglect. High AvgIG indicates that tokens act as stiff control variables, facilitating the learning of a precise generator distribution. Under a Gaussian residual model,  $\Delta I_t$  is proportional to the reduction in residual entropy (bits), serving as an operational measure of “usable information”.

**MC:** While AvgIG demands local steepness, MC demands “horizontal” flatness along the data manifold. We measure whether nearby images map to tokens connected by a low-loss path in the tokenizer’s token space. If the token space is fragmented, interpolating between valid tokens will pass through high-loss barriers (artifacts), making the space difficult for  $G$  to model.

**Definition.** We sample pairs  $(x^A, x^B)$  such that  $d_{\mathcal{X}}(x^A, x^B) \leq \epsilon$ , where  $d_{\mathcal{X}}$  is a distance measure defined by the image space and  $\epsilon$  is a hyperparameter and encode  $z^A = E(x^A)$  and  $z^B = E(x^B)$ . Let  $\gamma : [0, 1] \rightarrow \mathcal{Z}$  be a path connecting the tokens (linear interpolation),  $\gamma(t) = (1-t)z^A + tz^B$ . Instead of pixel-wise reconstruction error, we evaluate the path using a realism loss  $\mathcal{L}_{\psi}$  derived from an auxiliary density model  $p_{\psi}$  (where higher loss  $\mathcal{L}_{\psi}(x)$  indicates lower realism). We define the worst realism loss along the latent path,  $L_{\max} = \max_{t \in [0, 1]} \mathcal{L}_{\psi}(D(\gamma(t)))$ , and the best reference loss of the endpoints ( $L_{\text{ref}} = \min(\mathcal{L}_{\psi}(D(z^A)), \mathcal{L}_{\psi}(D(z^B)))$ ). We define the **pairwise mode connectivity** score as the ratio:

$$\text{MC}(x^A, x^B) = \frac{L_{\text{ref}}}{L_{\max} + \delta} \in [0, 1], \quad (3)$$

where  $\delta > 0$  ensures numerical stability. This score approaches 1 if the path never incurs a realism loss higher than the better endpoint (no barrier), and drops toward 0 if the path traverses high-loss regions (off-manifold artifacts). Finally, we report the dataset-level score by sampling different  $x^A$  and  $x^B$  from the dataset that  $d_{\mathcal{X}}(x^A, x^B) \leq \epsilon$ :

$$MC = \mathbb{E}[MC(x^A, x^B)]. \quad (4)$$

High MC indicates that the valid tokens region is geometrically smooth and connected, ensuring that compositional edits and generative interpolation remain on the natural image manifold.

### 3.3 Diffusion Decoder D

We train the tokenizer ( $E, D$ ) for reconstruction. Let  $z = E(x)$  and let  $x_t$  be the noisy image at diffusion step  $t$  under a fixed schedule, with  $\epsilon \sim \mathcal{N}(0, I)$ . The diffusion decoder  $D$  is a denoiser  $\epsilon_D = \epsilon_D(x_t, t; z)$  trained by the standard conditional denoising loss:

$$\mathcal{L}_{\text{tok}}(E, D) = \mathbb{E}_{x \sim \mathcal{D}} \left[ \|\epsilon - \epsilon_D(x_t, t; z)\|_2^2 \right]. \quad (5)$$

This objective optimizes reconstruction under the encoder manifold  $\mathcal{M}_E$ ; it does not directly enforce that good tokens form a learnable geometry or that tokens are evenly useful, motivating our metrics and the additional regularizers in COMPTok.

### 3.4 Aligning Tokenizer Training with Completeness and Learnability

Our evaluation suggests two properties of the tokenizer that matter for  $G$ : (i) tokens should carry usable information that effectively captures the information in the image, (ii) the set of tokens that decode to realistic images should be low-barrier which is crucial for the learnability of the token space. COMPTok adds objectives that directly target these properties while preserving reconstruction quality.

#### 3.4.1 Mutual-Information Token Supervision

To discourage token neglect, we introduce a recognition model  $Q_\phi(z | x)$  trained to recover tokens from images decoded by the tokenizer decoder. We optimize:

$$\mathcal{L}_{\text{MI}}(D, \phi) = - \sum_{k=1}^K \mathbb{E}_{\hat{x} \sim D(\cdot | z)} \left[ \log Q_\phi(z_k | \hat{x}) \right], \quad (6)$$

where  $D(\cdot | z)$  denotes sampling from the diffusion decoder conditioned on  $z$ . AvgIG measures how effectively reconstruction error can be reduced by moving in token space during latent optimization. If some tokens are ignored by  $D$ , then changing those coordinates has little effect on  $D(z)$ , yielding weak gradients and slow error reduction, i.e., low AvgIG. Mutual-information supervision prevents this failure mode by forcing  $D(\cdot | z)$  to produce images from which each  $z_k$  is predictable. Operationally, this increases the sensitivity of the decoded image to token perturbations, improving conditioning of latent optimization and thereby increasing AvgIG.

#### 3.4.2 Swap-Regularized Compositionality

To enforce learnable geometry under token composition, we train on swapped tokens. Given two images  $x^A, x^B$ , we extract their latent tokens as sequences of tokens,  $z^A = (z_1^A, \dots, z_K^A)$  and  $z^B = (z_1^B, \dots, z_K^B)$ . We form a swapped tokens  $z^{A \leftarrow B}$  by replacing a subset of tokens in  $z^A$  with corresponding tokens from  $z^B$  according to a swap mask or index set  $\mathcal{K}$ . For example, an interleaved swap might yield a mixed sequence:

$$z^{A \leftarrow B} = (z_1^A, z_2^B, z_3^A, \dots, z_K^B). \quad (7)$$

We decode a swapped sample  $\tilde{x} \sim D(\cdot | z^{A \leftarrow B})$  and apply the mutual-information token supervision objective to ensure the decoder respects the mixed composition:

$$\mathcal{L}_{\text{MI}}^{\text{swap}}(D, \phi) = - \sum_{k=1}^K \mathbb{E} \left[ \log Q_\phi(z_k^{A \leftarrow B} | \tilde{x}) \right]. \quad (8)$$

This objective explicitly expands the set of valid compositions and empirically increases MC.

Method	#Token	Dim.	VQ	rFID $\downarrow$	AvgIG $\uparrow$	MC $\uparrow$	Gen.	Model	Type	#Token	#Step	gFID $\downarrow$	IS $\uparrow$
<b>2D-grid tokenizers</b>													
MaskBit [35]	256	12	✓	1.61	0.33	0.68	MaskBit	Mask.	256	256	1.52	328.6	
MAR [19]	256	16	✗	1.22	0.36	0.70	MAR-L	Mask.	256	64	1.78	296.0	
VQGAN [9]	256	16	✓	7.94	0.19	0.59	Tam. Trans.	AR	256	256	5.20	280.3	
ViT-VQGAN [39]	1024	32	✓	1.28	0.20	0.58	VIM-L	AR	1024	1024	4.17	175.1	
RQ-VAE [17]	256	256	✓	3.20	0.18	0.57	RQ-Trans.	AR	256	64	3.80	323.7	
VAR [31]	680	32	✓	0.90	0.29	0.66	VAR-d16	VAR	680	10	3.30	274.4	
ImageFolder [20]	286	32	✓	0.80	0.31	0.67	VAR-d16	VAR	286	10	2.60	295.0	
LlamaGen [30]	256	8	✓	2.19	0.17	0.44	LlamaGen-L	AR	256	256	3.80	248.3	
CRT [26]	256	8	✓	2.36	0.32	0.66	LlamaGen-L	AR	256	256	2.75	265.2	
Causal MAR [19]	256	16	✗	1.22	0.29	0.64	MAR-L	AR	256	256	4.07	232.4	
<b>1D token-sequence tokenizers</b>													
TiTok-S-128 [42]	128	16	✓	1.71	0.40	0.75	MaskGIT-L	Mask.	128	64	1.97	281.8	
TiTok-L-32 [42]	32	8	✓	2.21	0.27	0.62	MaskGIT-L	Mask.	32	8	2.77	194.0	
Semanticist [36]	256	16	✗	0.78	0.38	0.73	εLlamaGen-L	AR	32	32	2.57	260.9	
FlexTok [1]	256	18	✓	1.45	0.35	0.71	AR	AR	32	32	1.86	-	
<b>CompTok</b>	256	16	✗	1.27	0.43	0.74	εMaskGIT	Mask.	256	64	1.60	297.9	

**Table 1** Reconstruction and generation performance on ImageNet. “Dim.” denotes the dimension of the tokens, and “#Step” denotes the number of steps needed for generating the complete image. “#Token” stands for the number of tokens used for image reconstruction (left) and generation (right), respectively.

### 3.4.3 Manifold Constraint via Adversarial Flow Model (AFM)

Token swaps produce unpaired tokens  $z^{A \leftarrow B}$  that often decode to off-manifold artifacts, creating connectivity barriers between valid regions. To constrain these mixed tokens to the natural image manifold, we adopt the Adversarial Flow Model (AFM) [21] as a realism prior. We employ a time-conditioned discriminator  $D_\psi(x_t, t)$  trained via a relativistic objective to distinguish between real data flows and generated flows. The decoder D is optimized to fool the discriminator while maintaining deterministic transport stability via the following generator objective:

$$\mathcal{L}_{\text{AFM}}(D) = \underbrace{\mathbb{E}[\text{softplus}(D_\psi(x_t, t) - D_\psi(\tilde{x}_t, t))]}_{\text{Manifold Constraint (Realism)}} \quad (9)$$

$$+ \lambda_{\text{OT}} \underbrace{\mathbb{E}[\|\tilde{x} - x\|_2^2]}_{\text{Stability (OT)}}, \quad (10)$$

where  $\tilde{x}$  are decoded images (reconstructions of swapped tokens or non-swapped tokens) diffused to time  $t$ , and  $x$  are real targets (applied only when available). The adversarial term acts as a powerful manifold prior for swapped tokens  $z^{A \leftarrow B}$ : it penalizes any decode  $\tilde{x}$  that lies in low-density artifact regions, effectively pushing the decoder to map mixed tokens onto the natural image manifold defined by  $D_\psi$ . Simultaneously, the Optimal Transport (OT) term ensures the mapping remains straight and deterministic where targets exist. By forcing swapped decodes to be realistic, AFM eliminates the high-error barriers that typically separate valid tokens, thereby smoothing the latent geometry and directly increasing Mode Connectivity (MC).

COMPTOK is trained with a combined loss of the mutual information loss, the swapped mutual information loss, and the AFM loss.

### 3.5 Downstream Training of G: MaskGIT with a Diffusion Token Head

After training the tokenizer (E, D), we train a separate generator G on the tokenizer token space. Given  $x \sim \mathcal{D}$ , the encoder produces a continuous token sequence

$$z = E(x) = (z_1, \dots, z_K), \quad z_k \in \mathbb{R}^d. \quad (11)$$

*MaskGIT backbone.* We adopt MaskGIT to model masked token prediction via a bidirectional transformer  $G_\theta$ . For a random mask  $m \in \{0, 1\}^K$ , the backbone takes the visible tokens and mask indicators and outputs per-position context features:  $h_k = G_\theta(z_{-m}, m, c)_k$ .  $c$  is an optional conditioning signal (e.g., class label or text embedding).

Tokenizer	Remote Sensing				Medical				Text OCR			
	rFID↓	AvgIG↑	MC↑	Task↑	rFID↓	AvgIG↑	MC↑	Task↑	rFID↓	AvgIG↑	MC↑	Task↑
<b>2D-grid tokenizers</b>												
RAE [44]	146.1	0.130	0.47	75.9	160.7	0.124	0.46	59.3	131.5	0.121	0.49	76.0
VQGAN [9]	162.9	0.149	0.54	83.4	161.3	0.135	0.48	63.5	141.4	0.138	0.51	79.4
MAE [12]	135.3	0.147	0.54	85.1	155.4	0.141	0.54	62.0	134.3	0.137	0.54	80.4
SDXL VAE [24]	145.9	0.131	0.48	79.7	158.2	0.128	0.46	62.3	137.2	0.143	0.53	79.2
<b>1D token-sequence tokenizers</b>												
TiTok-L-32 [42]	157.0	0.159	0.64	86.5	174.1	0.131	0.60	63.5	143.6	0.160	0.66	87.6
Semanticist [36]	159.9	0.144	0.64	84.2	171.6	0.151	0.66	67.0	159.0	0.144	0.66	86.3
FlexTok [1]	154.8	0.154	0.63	86.7	160.8	0.162	0.66	71.6	155.3	0.163	0.65	87.8
<b>CompTok (ours)</b>	168.1	0.157	0.66	88.7	153.7	0.159	0.69	74.9	141.5	0.167	0.65	91.9
Original Image	-	-	-	89.5	-	-	-	76.5	-	-	-	92.5
<b>Correlation with Task Utility (Pearson r across tokenizers; higher is better)</b>												
r(rFID, Task)		0.48				-0.18				0.62		
r(AvgIG, Task)		0.93				0.91				0.92		
r(MC, Task)		0.87				0.86				0.94		

**Table 2 Cross-domain tokenizer diagnostics and task utility.** For each tokenizer, we report rFID and our two diagnostics (AvgIG, local MC) computed on (E, D), plus downstream task performance on decoded images (Remote Sensing: segmentation accuracy/mIoU; Medical: Dice/mIoU; OCR: accuracy). The bottom block reports Pearson correlations across tokenizers, showing AvgIG/MC correlate more strongly with task utility than rFID.

*Continuous tokens: diffusion regression head.* Since  $z_k$  are continuous, we replace the discrete softmax head with a small diffusion MLP head  $M_\psi$  that generates each masked token from noise conditioned on  $h_k$ . Using a standard forward noising process  $z_k^t = \alpha_t z_k^0 + \sigma_t \epsilon$ ,  $\epsilon \sim \mathcal{N}(0, I)$ , we train  $(G_\theta, M_\psi)$  to predict  $\epsilon$ :

$$\mathcal{L}_G(\theta, \psi) = \mathbb{E}_{z=E(x), m, t} \left[ \sum_{k: m_k=1} \|\epsilon - M_\psi(z_k^t, h_k, t)\|_2^2 \right]. \quad (12)$$

As this generator predicts  $\epsilon$  for each masked token, we term it as  $\epsilon$ MaskGIT. At inference,  $\epsilon$ MaskGIT iteratively refines a partially masked sequence for  $S$  steps: it masks uncertain positions, samples their token values using the diffusion head conditioned on  $h_k$ , and repeats until all tokens are filled, yielding  $\hat{z}$ . An image is then obtained by decoding with the tokenizer diffusion decoder:  $\hat{x} \sim D(\cdot | \hat{z})$ .

## 4 Experiments

Our experiments validate two claims: (i) COMPTOK improves tokenizer quality and downstream generation, and (ii) our two metrics, AvgIG and MC, predict downstream generation and task utility more reliably than rFID. Experiment details are presented in the appendix.

### 4.1 Comparisons with state-of-the-art tokenizers

We compare COMPTOK against a suite of state-of-the-art tokenizers spanning both (i) 2D grid tokenization methods and (ii) prior 1D token sequence approaches. For each tokenizer, we report rFID and our generator-free diagnostics (AvgIG and MC computed on (E, D)). The gFID of the downstream generator trained on the token space of the tokenizer is also reported. The results are shown in Table 1. COMPTOK yields a strong rFID and notably better AvgIG and MC than the state-of-the-art tokenizers. Additionally,  $\epsilon$ MaskGIT trained on COMPTOK tokens achieves the best gFID among the generator variants. This improvement indicates that COMPTOK combined with  $\epsilon$ MaskGIT can be considered as a strong tokenizer and a generator on ImageNet class-conditional generation. This improvement in gFID is not explained by rFID alone: we observe cases where tokenizers with similar (or even better) rFID underperform in gFID, for example, Semanticist [36] and FlexTok [1], consistent with the rFID–gFID mismatch reported in prior works [11, 38]. In the same time, we can observe that the AvgIG and MC of COMPTOK outperforms the tokenizers with similar rFIDs, which means that AvgIG and MC are more predictive of gFID than rFID.

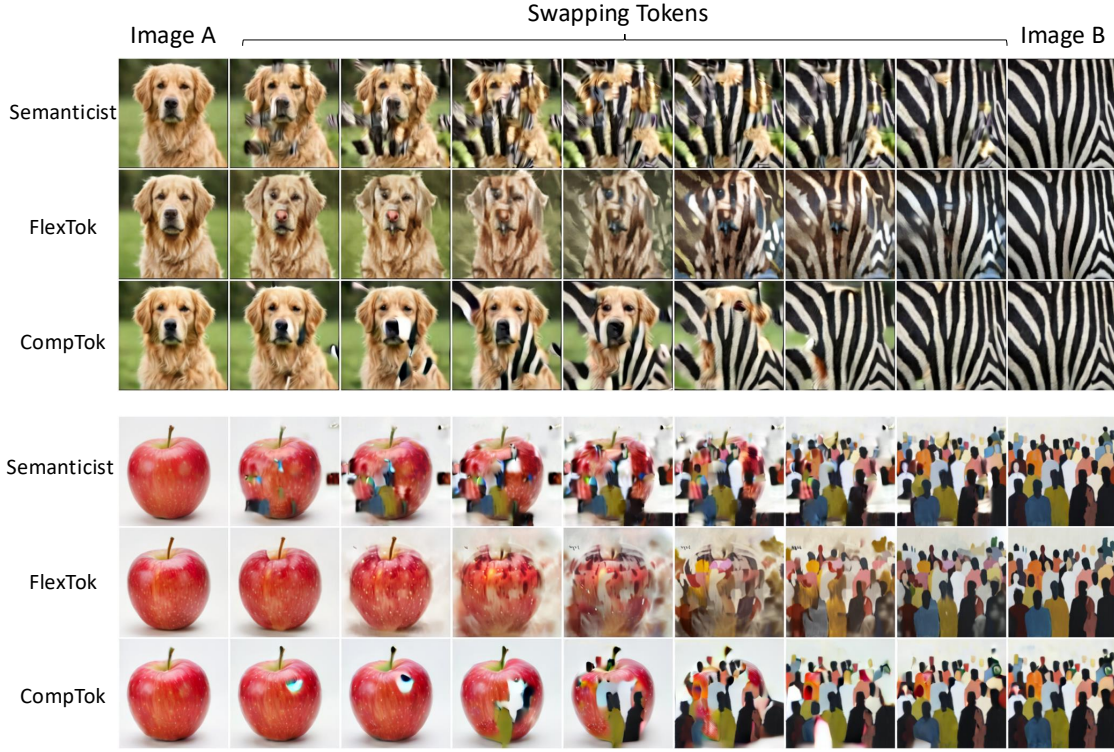


**Figure 3** Token swapping as a compositionality probe. For each row, we progressively swap an increasing subset of tokens from Image B into Image A. COMPTOK preserves coherent structure while transferring semantics, e.g., zebra stripes onto a dog; crowd appearance onto an apple, whereas baselines exhibit mixing artifacts and off-manifold blends.

## 4.2 Ablations

We ablate each of the three proposed training components in COMPTOK: (i) mutual-information token supervision  $\mathcal{L}_{\text{MI}}$ , (ii) swap-regularized recoverability  $\mathcal{L}_{\text{MI}}^{\text{swap}}$ , and (iii) the Adversarial Flow Model manifold constraint  $\mathcal{L}_{\text{AFM}}$ . For each ablation, we report AvgIG, local MC, rFID, and gFID using the same training budget.

The results are shown in Table 3. Removing  $\mathcal{L}_{\text{MI}}$  significantly reduces AvgIG: if tokens are not required to be recoverable from decoded samples, some token coordinates become weakly coupled to the decoder output, yielding poor conditioning and lower information gain during latent optimization. In contrast, rFID does not change that drastically, reflecting that encoder-manifold reconstruction alone does not enforce token usefulness.  $\mathcal{L}_{\text{MI}}^{\text{swap}}$  matters for MC as dropping it would increase the loss barrier between valid tokens. Removing

$\mathcal{L}_{\text{AFM}}$  also leads to a drop in MC. This aligns with the intuition that AFM provides an adversarial manifold constraint [21] that penalizes off-manifold generations, thereby smoothing the decoded landscape around swapped-token regions and reducing barriers. Again, rFID alone does not reliably predict these effects.

## 4.3 Correlations with Downstream Task Utility

A useful tokenizer should preserve relevant semantics under encode-decode, not just pixel-level similarity. Reconstruction metrics such as rFID can be dominated by low-level artifacts and may fail to reflect whether decoded images remain informative for downstream perception tasks. We therefore test whether AvgIG and MC correlate with task performance more strongly than rFID on three domains not only require pixel-level

Variant	rFID $\downarrow$	AvgIG $\uparrow$	MC $\uparrow$	gFID $\downarrow$
Full COMPTOK	1.27	0.43	0.74	1.60
w/o $\mathcal{L}_{\text{MI}}$	1.89	0.21	0.71	2.45
w/o $\mathcal{L}_{\text{MI}}^{\text{swap}}$	1.42	0.29	0.62	2.68
w/o $\mathcal{L}_{\text{AFM}}$	1.93	0.40	0.67	2.71

**Table 3 Ablations of CompTok on ImageNet.** We ablate each proposed loss term and report rFID, our metrics (AvgIG, MC), and downstream gFID after training the same  $\epsilon$ MaskGIT generator G on the resulting token space.

fidelity but also semantic accuracy. The three domains are (i) remote sensing, (ii) medical image understanding, and (iii) text OCR. We use datasets from DeepGlobe [5], ChestX-ray14 [15], and TextOCR [28] respectively for the three domains. For each tokenizer, we run an encode–decode pipeline using (E, D) and evaluate a fixed downstream task model on the decoded images using the task relevant metrics. We only used a subset of the full test set for each of the tasks to speed up the evaluation process. Results are presented in Table 2. Across tokenizers, AvgIG and MC correlate more strongly with task performance than rFID. This supports the interpretation that AvgIG/MC are sensitive to whether token spaces preserve usable semantic information: high AvgIG indicates that informative directions in latent token space remain accessible and stable, while high MC indicates that small semantic variations do not map to disconnected or brittle latent regions that would distort fine structures critical for segmentation and OCR. These results position AvgIG and MC as practical metrics for selecting tokenizers when the end goal is semantic utility, especially in domains where FID-style reconstruction metrics are known to be imperfect proxies.

#### 4.4 Qualitative Results

Figure 3 is a qualitative readout of the same two properties targeted by AvgIG and MC. Clean, stable partial swaps imply that many tokens have actionable influence rather than being ignored, which corresponds to higher AvgIG. Meanwhile, the absence of “broken” intermediate states indicates that mixed tokens lie in a connected low-barrier region under the realism criterion, aligning with higher MC. When baselines smear or collapse during partial swaps, COMPTOK is able to preserve a coherent scene layout while cleanly transferring attributes from Image B onto Image A, yielding realistic intermediate compositions and stable binding.

### 5 Conclusion

We presented COMPTOK, a diffusion-decoder visual tokenizer designed for downstream token-space generators, and introduced two metrics, AvgIG and MC, that better characterize token-space usefulness and learnability than the reconstruction-only metric of rFID. Empirically, AvgIG and MC correlate more strongly with downstream gFID and with semantic task utility across remote sensing, medical segmentation, and OCR settings. Guided by these metrics, COMPTOK combines mutual-information token supervision, token swapping-based compositional training, and an adversarial flow manifold constraint to reduce token neglect and keep mixed tokens on the real image manifold, yielding improved generation quality by providing a easier to learn latent space for the generator. Overall, our results suggest that evaluating and designing tokenizers should prioritize the geometry and usability of the induced token space, as captured by AvgIG and MC, rather than reconstruction fidelity alone.

### References

- [1] Roman Bachmann, Jesse Allardice, David Mizrahi, Enrico Fini, Oğuzhan Fatih Kar, Elmira Amirloo, Alaaeldin El-Nouby, Amir Zamir, and Afshin Dehghan. FlexTok: Resampling images into 1d token sequences of flexible length. *arXiv* 2025, 2025.
- [2] L Lao Beyer, Tianhong Li, Xinlei Chen, Sertac Karaman, and Kaiming He. Highly compressed tokenizer can generate without training. *arXiv preprint arXiv:2506.08257*, 2025.
- [3] Huiwen Chang, Han Zhang, Lu Jiang, Ce Liu, and William T. Freeman. MaskGIT: Masked generative image transformer. In *CVPR*, 2022.
- [4] Huiwen Chang, Han Zhang, Jarred Barber, Aaron Maschinot, Jose Lezama, Lu Jiang, Ming-Hsuan Yang, Kevin Patrick Murphy, William T. Freeman, Michael Rubinstein, Yuanzhen Li, and Dilip Krishnan. Muse: Text-to-image generation via masked generative Transformers. In *ICML*, 2023.
- [5] Ilke Demir, Krzysztof Koperski, David Lindenbaum, Guan Pang, Jing Huang, Saikat Basu, Forest Hughes, Devis Tuia, and Ramesh Raskar. Deepglobe 2018: A challenge to parse the earth through satellite images. In *Proceedings of the IEEE conference on computer vision and pattern recognition workshops*, pages 172–181, 2018.
- [6] Prafulla Dhariwal and Alex Nichol. Diffusion models beat GANs on image synthesis. In *NeurIPS*, 2021.

[7] Alexey Dosovitskiy, Lucas Beyer, Alexander Kolesnikov, Dirk Weissenborn, Xiaohua Zhai, Thomas Unterthiner, Mostafa Dehghani, Matthias Minderer, Georg Heigold, Sylvain Gelly, Jakob Uszkoreit, and Neil Houlsby. An image is worth 16x16 words: Transformers for image recognition at scale. In ICLR, 2021.

[8] Shivam Duggal, Phillip Isola, Antonio Torralba, and William T. Freeman. Adaptive length image tokenization via recurrent allocation. In ICLR, 2025.

[9] Patrick Esser, Robin Rombach, and Bjorn Ommer. Taming Transformers for high-resolution image synthesis. In CVPR, 2021.

[10] Yuying Ge, Yixiao Ge, Ziyun Zeng, Xintao Wang, and Ying Shan. Planting a seed of vision in large language model. arXiv:2307.08041, 2023.

[11] Philippe Hansen-Estruch, David Yan, Ching-Yao Chung, Orr Zohar, Jialiang Wang, Tingbo Hou, Tao Xu, Sriram Vishwanath, Peter Vajda, and Xinlei Chen. Learnings from scaling visual tokenizers for reconstruction and generation. arXiv:2501.09755, 2025.

[12] Kaiming He, Xinlei Chen, Saining Xie, Yanghao Li, Piotr Dollár, and Ross Girshick. Masked autoencoders are scalable vision learners. In CVPR, 2022.

[13] Martin Heusel, Hubert Ramsauer, Thomas Unterthiner, Bernhard Nessler, and Sepp Hochreiter. GANs trained by a two time-scale update rule converge to a local Nash equilibrium. In NeurIPS, 2017.

[14] Jonathan Ho, Ajay Jain, and Pieter Abbeel. Denoising diffusion probabilistic models. In NeurIPS, 2020.

[15] Jeremy Irvin, Pranav Rajpurkar, Michael Ko, Yifan Yu, Silviana Ciurea-Ilcus, Chris Chute, Henrik Marklund, Behzad Haghgoo, Robyn Ball, Katie Shpanskaya, et al. Chexpert: A large chest radiograph dataset with uncertainty labels and expert comparison. In Proceedings of the AAAI conference on artificial intelligence, volume 33, pages 590–597, 2019.

[16] Diederik P. Kingma and Max Welling. Auto-encoding variational bayes. In ICLR, 2014.

[17] Doyup Lee, Chiheon Kim, Saehoon Kim, Minsu Cho, and Wook-Shin Han. Autoregressive image generation using residual quantization. In CVPR, 2022.

[18] Tianhong Li, Dina Katabi, and Kaiming He. Return of unconditional generation: A self-supervised representation generation method. In NeurIPS, 2024.

[19] Tianhong Li, Yonglong Tian, He Li, Mingyang Deng, and Kaiming He. Autoregressive image generation without vector quantization. In NeurIPS, 2024.

[20] Xiang Li, Kai Qiu, Hao Chen, Jason Kuen, Jiuxiang Gu, Bhiksha Raj, and Zhe Lin. Imagefolder: Autoregressive image generation with folded tokens. In ICLR, 2025.

[21] Shanchuan Lin, Ceyuan Yang, Zhijie Lin, Hao Chen, and Haoqi Fan. Adversarial flow models. arXiv preprint arXiv:2511.22475, 2025.

[22] Maxime Oquab, Timothée Darcet, Theo Moutakanni, Huy V. Vo, Marc Szafraniec, Vasil Khalidov, Pierre Fernandez, Daniel Haziza, Francisco Massa, Alaeldin El-Nouby, Russell Howes, Po-Yao Huang, Hu Xu, Vasu Sharma, Shang-Wen Li, Wojciech Galuba, Mike Rabbat, Mido Assran, Nicolas Ballas, Gabriel Synnaeve, Ishan Misra, Herve Jegou, Julien Mairal, Patrick Labatut, Armand Joulin, and Piotr Bojanowski. DINOv2: Learning robust visual features without supervision. TMLR, 2024.

[23] William Peebles and Saining Xie. Scalable diffusion models with transformers. In ICCV, 2023.

[24] Dustin Podell, Zion English, Kyle Lacey, Andreas Blattmann, Tim Dockhorn, Jonas Müller, Joe Penna, and Robin Rombach. Sdxl: Improving latent diffusion models for high-resolution image synthesis. arXiv preprint arXiv:2307.01952, 2023.

[25] Alec Radford, Jong Wook Kim, Chris Hallacy, Aditya Ramesh, Gabriel Goh, Sandhini Agarwal, Girish Sastry, Amanda Askell, Pamela Mishkin, Jack Clark, Gretchen Krueger, and Ilya Sutskever. Learning transferable visual models from natural language supervision. In ICML, 2021.

[26] Vivek Ramanujan, Kushal Tirumala, Armen Aghajanyan, Luke Zettlemoyer, and Ali Farhadi. When worse is better: Navigating the compression-generation tradeoff in visual tokenization. arXiv:2412.16326, 2024.

[27] Robin Rombach, Andreas Blattmann, Dominik Lorenz, Patrick Esser, and Björn Ommer. High-resolution image synthesis with latent diffusion models. In CVPR, 2022.

[28] Amanpreet Singh, Guan Pang, Mandy Toh, Jing Huang, Wojciech Galuba, and Tal Hassner. Textocr: Towards large-scale end-to-end reasoning for arbitrary-shaped scene text. In Proceedings of the IEEE/CVF conference on computer vision and pattern recognition, pages 8802–8812, 2021.

[29] Jiaming Song, Chenlin Meng, and Stefano Ermon. Denoising diffusion implicit models. In ICLR, 2021.

[30] Peize Sun, Yi Jiang, Shoufa Chen, Shilong Zhang, Bingyue Peng, Ping Luo, and Zehuan Yuan. Autoregressive model beats diffusion: Llama for scalable image generation. arXiv:2406.06525, 2024.

[31] Keyu Tian, Yi Jiang, Zehuan Yuan, Bingyue Peng, and Liwei Wang. Visual autoregressive modeling: Scalable image generation via next-scale prediction. In NeurIPS, 2024.

[32] Aäron van den Oord, Nal Kalchbrenner, and Koray Kavukcuoglu. Pixel recurrent neural networks. In ICML, 2016.

[33] Aäron van den Oord, Nal Kalchbrenner, Oriol Vinyals, Lasse Espeholt, Alex Graves, and Koray Kavukcuoglu. Conditional image generation with PixelCNN decoders. In NeurIPS, 2016.

[34] Aäron van den Oord, Oriol Vinyals, and Koray Kavukcuoglu. Neural discrete representation learning. In NeurIPS, 2017.

[35] Mark Weber, Lijun Yu, Qihang Yu, Xueqing Deng, Xiaohui Shen, Daniel Cremers, and Liang-Chieh Chen. MaskBit: Embedding-free image generation via bit tokens. TMLR, 2024.

[36] Xin Wen, Bingchen Zhao, Ismail Elezi, Jiankang Deng, and Xiaojuan Qi. “Principal components” enable a new language of images. In IEEE/CVF International Conference on Computer Vision (ICCV), 2025.

[37] Jingfeng Yao and Xinggang Wang. Reconstruction vs. generation: Taming optimization dilemma in latent diffusion models. arXiv:2501.01423, 2025.

[38] Jingfeng Yao, Bin Yang, and Xinggang Wang. Reconstruction vs. generation: Taming optimization dilemma in latent diffusion models. In Proceedings of the Computer Vision and Pattern Recognition Conference, pages 15703–15712, 2025.

[39] Jiahui Yu, Xin Li, Jing Yu Koh, Han Zhang, Ruoming Pang, James Qin, Alexander Ku, Yuanzhong Xu, Jason Baldridge, and Yonghui Wu. Vector-quantized image modeling with improved VQGAN. In ICLR, 2022.

[40] Lijun Yu, José Lezama, Nitesh B. Gundavarapu, Luca Versari, Kihyuk Sohn, David Minnen, Yong Cheng, Vighnesh Birodkar, Agrim Gupta, Xiuye Gu, Alexander G. Hauptmann, Boqing Gong, Ming-Hsuan Yang, Irfan Essa, David A. Ross, and Lu Jiang. Language model beats diffusion – tokenizer is key to visual generation. In ICLR, 2024.

[41] Qihang Yu, Ju He, Xueqing Deng, Xiaohui Shen, and Liang-Chieh Chen. Randomized autoregressive visual generation. arXiv:2411.00776, 2024.

[42] Qihang Yu, Mark Weber, Xueqing Deng, Xiaohui Shen, Daniel Cremers, and Liang-Chieh Chen. An image is worth 32 tokens for reconstruction and generation. In NeurIPS, 2024.

[43] Sihyun Yu, Sangkyung Kwak, Huiwon Jang, Jongheon Jeong, Jonathan Huang, Jinwoo Shin, and Saining Xie. Representation alignment for generation: Training diffusion transformers is easier than you think. In ICLR, 2025.

[44] Boyang Zheng, Nanye Ma, Shengbang Tong, and Saining Xie. Diffusion transformers with representation autoencoders. arXiv preprint arXiv:2510.11690, 2025.

[45] Lei Zhu, Fangyun Wei, Yanye Lu, and Dong Chen. Scaling the codebook size of VQ-GAN to 100,000 with a utilization rate of 99%. In NeurIPS, 2024.

# Appendix

## A Implementation Details

*COMPTOK autoencoder.* The encoder of COMPTOK is a standard ViT-B/16 [7], except for additional concept tokens and causal attention masks applied to them. Before being fed to the decoder, the concept tokens are normalized by their own mean and variance following [18]. The decoder is a DiT [23] with a patch size of 2. We take DiT-L as default following Wen et al. [36]. The decoder operates on the latent space of a publicly available KL-16 VAE provided by [19] to reduce computation cost. The VAE is frozen during training, and both the encoder and decoder are trained from scratch. To enforce the quality of the learned concept tokens and stabilize training, we apply REPA [43] with DINoV2-B [22] as a regularizer to the 8th layer of the DiT decoder. We do not apply weighting on the loss terms of  $\mathcal{L}_{\text{tok}}$ ,  $\mathcal{L}_{\text{MI}}$ ,  $\mathcal{L}_{\text{MI}}^{\text{swap}}$ , and  $\mathcal{L}_{\text{AFM}}$ , as we found this yield the best performance.

*Autoregressive image modeling.* We validate the effectiveness of COMPTOK autoencoder by training autoregressive image generation models using MaskGIT [3] combined with diffusion loss [19]. The input sequence is pre-pended with a [CLS] token for class conditioning, which is randomly dropped out with probability 0.1 during training for classifier-free guidance. At inference time, we use a CFG schedule following [4, 19], and do not apply temperature sampling. Note that the implementation can be general. While our preliminary validation demonstrates promising results, we anticipate better configurations in future work.

*AvgIG.* We fix the decoder and, for each evaluation image, initialize  $z^0$  from a random latent of the appropriate shape. We run 100 steps of gradient descent on  $\frac{1}{2}\|D(z) - x\|_2^2$  with step size  $\eta = 0.001$ . We record  $\text{MSE}_t$  and compute  $\Delta I_t(x) = \frac{N}{2} \log_2 (\text{MSE}_t / \text{MSE}_{t+1})$  at each step, then average over steps and images. We use a small numerical floor on MSE to avoid division by zero.

*MC.* We set  $\mathcal{L} * \psi(x)$  to be the realism loss induced by the adversarial flow model [21] trained via  $\mathcal{L} * \text{AFM}$ . On ImageNet, we construct “nearby” pairs using CLIP image embeddings: for each anchor image, we select (i) the nearest neighbor within the same class and (ii) the nearest neighbor from a different class. We report the average MC over all evaluated pairs.

## B Additional Qualitative Results on Token Swapping

Figure 4,5,6,7,8 presents more qualitative results on swapping tokens between images. From the top row the bottom row of these figures, we present the results of swapping tokens on MaskBit [35], a 2D tokenizer, Semanticist [36], FlexTok [1], and COMPTOK. We can observe the improved ability of mixing semantics of COMPTOK comparing to other models.

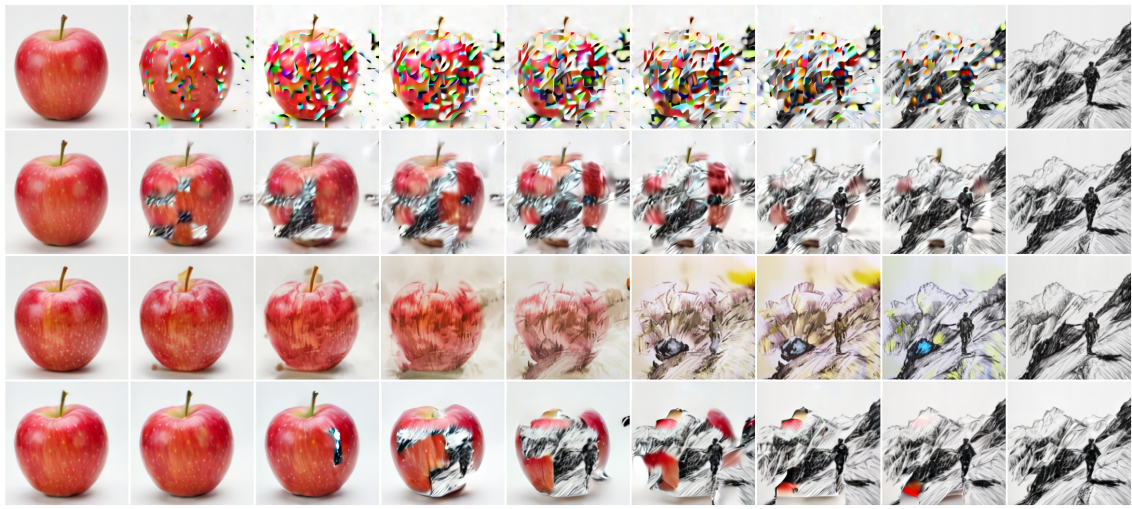


Figure 4



Figure 5



Figure 6

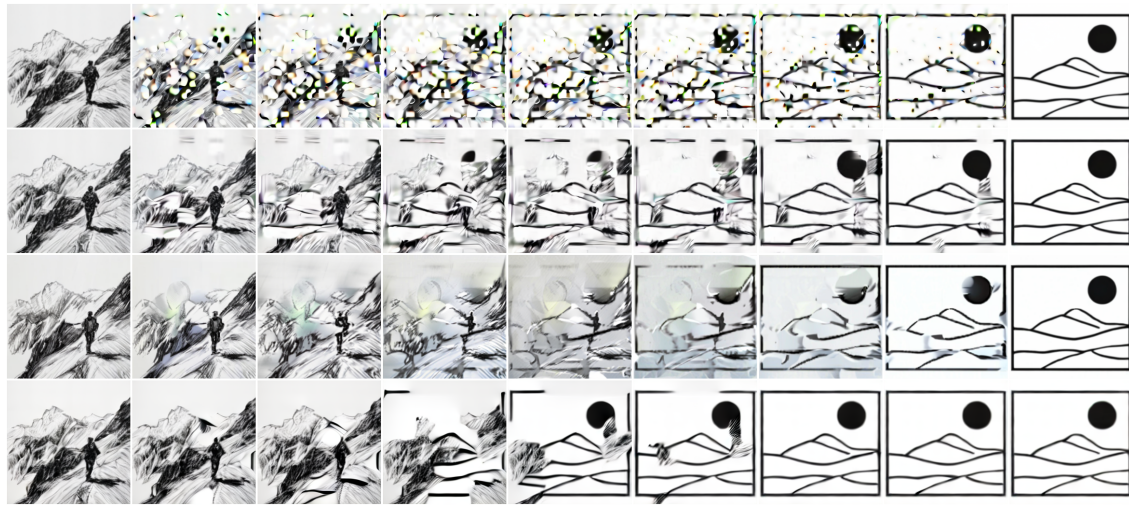


Figure 7

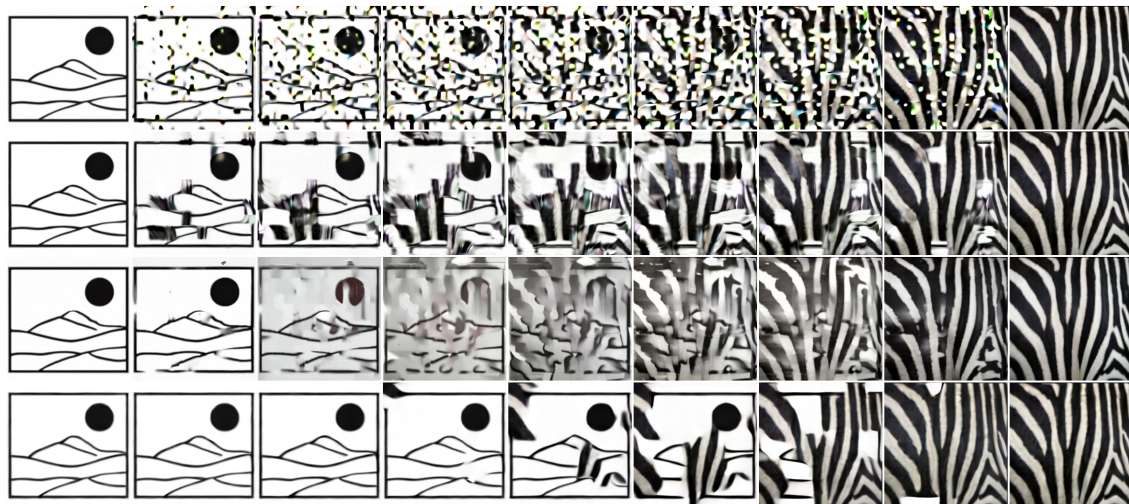


Figure 8

## C Operational Definitions and Guarantees for AvgIG and Local MC

This appendix provides a formal treatment of the two diagnostics introduced in the main text—**AvgIG** (Average Information Gain) and **MC** (Mode Connectivity). We provide precise definitions, prove their theoretical interpretations, and formally demonstrate how the proposed training objectives ( $\mathcal{L}_{\text{MI}}$ ,  $\mathcal{L}_{\text{swap}}$ , and  $\mathcal{L}_{\text{AFM}}$ ) act to optimize these metrics.

### C.1 Setup and Notation

Let  $(E, D)$  be a tokenizer where  $E : \mathcal{X} \rightarrow \mathcal{Z}$  maps images to a token space  $\mathcal{Z} \subset \mathbb{R}^{K \times d}$  (represented as continuous embeddings before quantization or strictly continuous tokens), and  $D : \mathcal{Z} \rightarrow \mathcal{X}$  is a generator/decoder. We assume the decoder output  $D(z)$  represents the mean of a probabilistic decoding distribution or a deterministic mapping.

**Realism Loss.** Let  $\mathcal{L}_\psi : \mathcal{X} \rightarrow \mathbb{R}_{\geq 0}$  be a differentiable realism loss function derived from an auxiliary density model  $p_\psi(x)$ , such that  $\mathcal{L}_\psi(x) = -\log p_\psi(x) + C$ . Lower values indicate higher realism.

**Latent Space Optimization (LSO).** Given a target image  $x$ , we define the optimization trajectory  $\mathcal{T}_x = \{z_t\}_{t=0}^T$  generated by gradient descent on the Mean Squared Error (MSE) reconstruction loss:

$$z_0 = E(x), \quad z_{t+1} = z_t - \eta \nabla_z \mathcal{L}_{\text{rec}}(D(z_t), x), \quad \text{where } \mathcal{L}_{\text{rec}}(x, y) = \frac{1}{2} \|x - y\|_2^2. \quad (13)$$

**Nearby Pairs.** Let  $\mathcal{P}_\epsilon = \{(x^A, x^B) \in \mathcal{X}^2 : \|x^A - x^B\|_2 \leq \epsilon\}$  be the set of  $\epsilon$ -nearby image pairs.

### C.2 Operational Definitions

**Definition C.1** (AvgIG: Usable Information Gain). For a target  $x$  and optimization trajectory  $\{z_t\}$ , the per-step information gain (in bits) is defined as:

$$\Delta I_t(x) = \frac{N}{2} \log_2 \left( \frac{\mathcal{L}_{\text{rec}}(D(z_t), x)}{\mathcal{L}_{\text{rec}}(D(z_{t+1}), x)} \right), \quad (14)$$

where  $N$  is the data dimensionality (number of pixels). The system-level **AvgIG** is the expected gain over the data distribution and optimization steps:

$$\text{AvgIG} = \mathbb{E}_{x \sim p_{\text{data}}} \left[ \frac{1}{T} \sum_{t=0}^{T-1} \Delta I_t(x) \right]. \quad (15)$$

**Definition C.2** (Local MC: Pairwise Connectivity Ratio). For a pair  $(x^A, x^B) \in \mathcal{P}_\epsilon$ , let  $z^A, z^B$  be their tokens. Define the linear interpolation path  $\gamma(u) = (1 - u)z^A + uz^B$  for  $u \in [0, 1]$ . We define the Reference Loss ( $L_{\text{ref}}$ ) and the Path Maximum Loss ( $L_{\text{max}}$ ) using the realism function  $\mathcal{L}_\psi$ :

$$L_{\text{ref}}(x^A, x^B) = \min \left( \mathcal{L}_\psi(D(z^A)), \mathcal{L}_\psi(D(z^B)) \right), \quad (16)$$

$$L_{\text{max}}(x^A, x^B) = \max_{u \in [0, 1]} \mathcal{L}_\psi(D(\gamma(u))). \quad (17)$$

The Pairwise Mode Connectivity score is the ratio:

$$MC(x^A, x^B) = \frac{L_{\text{ref}}}{L_{\text{max}} + \delta}, \quad \delta > 0. \quad (18)$$

The system-level **MC** is  $\mathbb{E}_{(x^A, x^B) \sim \mathcal{P}_\epsilon} [MC(x^A, x^B)]$ .

### C.3 Theoretical Guarantees for Diagnostics

Here we provide formal justification for why these metrics capture “optimization condition” and “manifold smoothness”.

#### C.3.1 AvgIG Represents Likelihood Improvement

**Lemma C.3** (AvgIG  $\equiv$  Likelihood Gradient). *Assume a Gaussian probabilistic decoder  $p(x|z) = \mathcal{N}(x; D(z), \sigma^2 I)$ . Then, the term  $\Delta I_t(x)$  is exactly equal to the increase in log-likelihood of the target  $x$  achieved by the update step  $z_t \rightarrow z_{t+1}$  (shifted by a constant).*

*Proof.* The log-likelihood is  $\log p(x|z) = -\frac{N}{2} \log(2\pi\sigma^2) - \frac{1}{2\sigma^2} \|D(z) - x\|_2^2$ . The improvement in log-likelihood (in bits, base 2) is:

$$\Delta LL = \log_2 p(x|z_{t+1}) - \log_2 p(x|z_t) \quad (19)$$

$$= \frac{1}{2\sigma^2 \ln 2} \left( \|D(z_t) - x\|_2^2 - \|D(z_{t+1}) - x\|_2^2 \right). \quad (20)$$

Definition C.1 uses the ratio of MSEs. Note that for small steps,  $\log(a/b) = \log(1 + \frac{a-b}{b}) \approx \frac{a-b}{b}$ . AvgIG is a robust, scale-invariant formulation of this likelihood ascent. **Implication:** High AvgIG guarantees that the latent space provides actionable gradients that rapidly increase the data likelihood. If AvgIG is low, the decoder is locally invariant to the token (vanishing gradients) or the loss landscape is ill-conditioned.  $\square$

#### C.3.2 Smoothness Implies High MC

We formally prove that geometric smoothness of the realism landscape implies an MC score close to 1.

**Theorem C.4** (Lipschitz Smoothness Lower Bounds MC). *Let  $\mathcal{L}_{real}(z) := \mathcal{L}_\psi(D(z))$  be the composition of the decoder and realism loss. Assume  $\mathcal{L}_{real}$  is K-Lipschitz continuous on the convex hull of the token space:  $|\mathcal{L}_{real}(z) - \mathcal{L}_{real}(z')| \leq K\|z - z'\|_2$ . Then, for any pair  $(x^A, x^B)$  with token distance  $\Delta_z = \|z^A - z^B\|_2$ :*

$$MC(x^A, x^B) \geq \frac{1}{1 + \frac{K\Delta_z + |d_{end}|}{L_{ref} + \delta}}, \quad (21)$$

where  $d_{end} = \mathcal{L}_{real}(z^A) - \mathcal{L}_{real}(z^B)$  is the endpoint discrepancy.

*Proof.* Let  $\gamma(u) = (1 - u)z^A + uz^B$ . By Lipschitz continuity:

$$L_{max} = \max_{u \in [0, 1]} \mathcal{L}_{real}(\gamma(u)) \quad (22)$$

$$\leq \mathcal{L}_{real}(z^A) + \max_u K\|\gamma(u) - z^A\|_2 \quad (23)$$

$$= \mathcal{L}_{real}(z^A) + K\|z^B - z^A\|_2. \quad (24)$$

Without loss of generality, assume  $\mathcal{L}_{real}(z^A) \leq \mathcal{L}_{real}(z^B)$ , so  $L_{ref} = \mathcal{L}_{real}(z^A)$ . Then  $L_{max} \leq L_{ref} + K\Delta_z + (\mathcal{L}_{real}(z^B) - \mathcal{L}_{real}(z^A))$  if we started from the larger endpoint, but strictly bounded by  $L_{ref} + K\Delta_z$  relative to the start point. Taking the conservative bound  $L_{max} \leq L_{ref} + K\Delta_z + |d_{end}|$ , we substitute into the MC definition:

$$MC = \frac{L_{ref}}{L_{max} + \delta} \geq \frac{L_{ref}}{L_{ref} + K\Delta_z + |d_{end}| + \delta} = \frac{1}{1 + \frac{K\Delta_z + |d_{end}|}{L_{ref} + \delta}}. \quad (25)$$

$\square$

**Implication:** As token distance  $\Delta_z \rightarrow 0$  (which is true for nearby images in a continuous encoder), MC approaches 1. Low MC values prove the violation of the Lipschitz condition—i.e., the existence of sharp, high-loss barriers (“spikes” or “holes”) in the latent manifold.

## C.4 Connecting Proposed Losses to Diagnostics

We now formally demonstrate how our training objectives optimize these diagnostics.

### C.4.1 Why Mutual Information ( $\mathcal{L}_{\text{MI}}$ ) Improves AvgIG

**Proposition C.5** (MI Maximization Enforces Non-Zero Gradients). *Let the decoder be  $p_\theta(x|z)$ . The gradients used in LSO are  $\nabla_z \log p_\theta(x|z)$ . Minimizing the MI loss  $\mathcal{L}_{\text{MI}}$  effectively maximizes a lower bound on the gradient norms  $\|\nabla_z \log p_\theta(x|z)\|$ .*

*Proof.* The InfoGAN-style loss is  $\mathcal{L}_{\text{MI}} \approx -\mathbb{E}_{z,x \sim D(z)}[\log q_\phi(z|x)]$ . This optimizes a variational lower bound on the Mutual Information  $I(Z; X)$ . Consider the Fisher Information formulation. High mutual information implies that  $Z$  strongly predicts  $X$ . If the decoder were locally invariant to a token dimension  $z_k$  (i.e.,  $\nabla_{z_k} D(z) \approx 0$ ), then changing  $z_k$  would not change  $x$ , making  $x$  uninformative about  $z_k$ . This results in  $I(Z_k; X) \approx 0$  and high  $\mathcal{L}_{\text{MI}}$ . Conversely, minimizing  $\mathcal{L}_{\text{MI}}$  forces  $I(Z; X)$  to be high, which requires the decoder to be sensitive to changes in  $z$ . Sensitivity is mathematically equivalent to  $\mathbb{E}[\|\nabla_z D(z)\|^2] > 0$ . Since AvgIG is driven by the magnitude of the gradient  $\nabla_z \mathcal{L}_{\text{rec}}$ , ensuring non-zero sensitivity directly increases AvgIG.  $\square$

### C.4.2 Why Swap Training ( $\mathcal{L}_{\text{swap}}$ ) Improves Local MC

**Proposition C.6** (Swap Training Bounds Path Loss). *Let  $z^{\text{swap}}$  be a token formed by swapping tokens between  $z^A$  and  $z^B$ .  $z^{\text{swap}}$  lies on the boundary of the hyper-rectangle defined by  $z^A, z^B$ . Minimizing  $\mathcal{L}_{\text{rec}}^{\text{swap}}(z^{\text{swap}})$  minimizes the realism loss at intermediate points along the interpolation path  $\gamma(u)$ .*

*Proof.* The MC metric penalizes  $L_{\text{max}} = \max_u \mathcal{L}_\psi(D(\gamma(u)))$ . While  $\gamma(u)$  is a continuous diagonal path, the swapped token  $z^{\text{swap}}$  represents a “vertex” move on the hypercube between  $z^A$  and  $z^B$ . Let  $\mathcal{S}_{AB}$  be the set of all token-swapped tokens between  $z^A$  and  $z^B$ . Swap training minimizes  $\mathbb{E}_{z \in \mathcal{S}_{AB}}[\mathcal{L}_{\text{rec}}(z)]$ . Assuming the decoder is smooth (locally Lipschitz with constant  $K$ ), the loss at any point  $\gamma(u)$  on the diagonal is bounded by the loss at the nearest swapped vertices. Specifically, for any  $u$ , there exists a  $z^{\text{swap}}$  such that  $\|\gamma(u) - z^{\text{swap}}\|$  is small. By minimizing the loss at the dense set of swapped vertices  $\mathcal{S}_{AB}$ , we lower the upper bound of the loss surface over the entire region, thereby reducing  $L_{\text{max}}$  and increasing the MC ratio.  $\square$

### C.4.3 Why AFM ( $\mathcal{L}_{\text{AFM}}$ ) Improves Local MC

**Proposition C.7** (Adversarial Alignment Minimizes  $L_{\text{max}}$ ). *The AFM objective minimizes the Jensen-Shannon divergence (or equivalent adversarial metric) between the distribution of swapped decodes  $P_{\text{swap}}$  and real data  $P_{\text{data}}$ . Minimizing  $\mathcal{L}_{\text{AFM}}$  implies  $P_{\text{swap}} \rightarrow P_{\text{data}}$  in distribution. This maximizes the expected MC score.*

*Proof.* Recall the MC definition relies on  $L_{\text{max}}$ , the maximum realism loss (inverse likelihood) along the path. High  $L_{\text{max}}$  corresponds to “off-manifold” artifacts (low probability under  $P_{\text{data}}$ ). The adversarial generator loss is:

$$\min_D \mathcal{L}_{\text{adv}} = \min_D \mathbb{E}_{z \sim \text{Swaps}}[\text{softplus}(D_\psi(D(z)) - D_\psi(x))]. \quad (26)$$

The global optimum of this objective is achieved when the distribution of generated swapped images exactly matches the real data distribution ( $P_{\text{swap}} = P_{\text{data}}$ ). If  $P_{\text{swap}} = P_{\text{data}}$ , then the support of swapped decodes lies entirely within the high-density region of real images. Consequently, for any swapped token  $z^{\text{swap}}$  (which lies near the interpolation path), the realism loss  $\mathcal{L}_\psi(D(z^{\text{swap}}))$  is minimized (approaching the loss of real data). This minimizes the denominator  $L_{\text{max}} + \delta$  in the MC ratio, pushing the MC score towards its theoretical maximum of 1.  $\square$